

Article

Synthesis, Characterization, and Biological Evaluation of Red-Absorbing Fe(II) Polypyridine Complexes

Johannes Karges ¹, Philippe Goldner ² and Gilles Gasser ^{1,*}

¹ Laboratory for Inorganic Chemical Biology, Chimie ParisTech, PSL University, 75005 Paris, France; johannes.karges@chimieparistech.psl.eu

² Chimie ParisTech, PSL University, CNRS, Institut de Recherche de Chimie Paris, 75005 Paris, France; philippe.goldner@chimieparistech.psl.eu

* Correspondence: gilles.gasser@chimieparistech.psl.eu; Tel.: +33-1-44-27-56-02

Received: 7 December 2018; Accepted: 28 December 2018; Published: 7 January 2019



Abstract: Cancer is known to be one of the major causes of death nowadays. Among others, chemotherapy with cisplatin is a commonly used treatment. Although widely employed, cisplatin is known to cause severe side effects, such as nerve and kidney damage, nausea, vomiting, and bone marrow suppression. Most importantly, a number of cancer tumors are acquiring resistance to cisplatin, limiting its clinical use. There is therefore a need for the discovery of novel anticancer agents. Complementary to chemotherapy, Photodynamic Therapy (PDT) has expanded the range of treatment opportunities of numerous kinds of cancer. Nonetheless, the currently approved PDT photosensitizers (PSs) suffer from major drawbacks, which include poor water solubility or photobleaching, in addition to a slow clearance from the body that causes photosensitivity. Due to these limitations, there is a need for the development of new PDT PSs. To overcome these problems, a lot of research groups around the world are currently focusing their attention towards the development of new metal complexes as PDT PSs. However, most synthesized compounds reported so far show limited use due to their poor absorption in the phototherapeutic window. Herein, we report on the preparation and characterization of three Fe(II) polypyridine complexes (**4–6**) and evaluate their potential as both anticancer agents and PDT PSs. Very importantly, these compounds are stable in human plasma, photostable upon continuous LED irradiation, and absorb in the red region of the spectrum. We could demonstrate that through additional sulfonic acid groups on the polypyridine ligand being used (bphen: 4,7-diphenyl-1,10-phenanthroline), the water solubility of the complexes could be highly improved, whereas the photophysical properties did not significantly change. One of these complexes (**4**) shows interesting toxicity, with IC₅₀ values in the low micromolar range in the dark as well as some phototoxicity upon irradiation at 480 and 540 nm against RPE-1 and HeLa cells.

Keywords: anticancer; medicinal inorganic chemistry; metals in medicine; photodynamic therapy

1. Introduction

Over the last decades, cancer has emerged as one of the deadliest diseases worldwide. Classical treatments are chemotherapy, surgery, radiotherapy, and immunotherapy. To efficiently treat tumors, a combination of these techniques is most commonly used [1,2]. Although cisplatin is still the most commonly used chemotherapeutic drug against cancer, it is responsible for a number of severe side-effects (e.g., nerve and kidney damage, nausea, vomiting, and bone marrow suppression). Additionally, a number of cancer tumors are acquiring resistance to cisplatin, limiting its clinical use. There is therefore a need for the development of new chemotherapeutic drug candidates. To tackle

this issue, the use of metal-based complexes is intensively studied due to their large structural variety as well as the possibility of ligand exchange or biological redox reactions [3–5]. Most research so far has been made on the metals Pt and Ru [6–13].

Complementary to chemotherapy, Photodynamic Therapy (PDT) has expanded the range of treatment opportunities of numerous kinds of cancer. This method is already approved to treat different kinds of cancer as well as other bacterial, fungal, or viral infections. Typically, during a PDT treatment, a preferably non-toxic photosensitizer (PS) is selectively activated upon light irradiation to create reactive oxygen species (ROS). More specially, the excited state of the PS is able to transfer electrons or protons from/to the biological environment to generate radicals or to transfer its energy to molecular oxygen generating singlet oxygen ($^1\text{O}_2$). So far, most of the research has been performed on PSs with a tetrapyrrolic scaffold. However, based on their similar structures, these compounds suffer from similar drawbacks (e.g., poor water solubility, photobleaching or a slow clearance from the body that causes photosensitivity) [14,15]. To overcome these limitations, metal complexes are currently investigated as alternatives to chlorins, phthalocyanines, or porphyrins due to their attractive physico-chemical properties (i.e., high water solubility, high chemical stability and photostability, high $^1\text{O}_2$ production) [16–19]. The most commonly studied transition metals in this field of research are Ru(II) [18,20–23], Os(II) [24,25], Rh(III) [26,27], and Ir(III) [28–30] complexes. However, these metals are not abundant. It would therefore be extremely interesting to develop a class of PDT PSs based on cheap, abundant metals. In this perspective, we have recently investigated the potential of easy-to-synthesize Cr(III) complexes as PDT PSs [31]. There have also been made some efforts in the design of Fe-based complexes. However, it is well established that Fe(II) polypyridine complexes are generally poorly emissive with very short lifetimes. This is the case due to the fast depopulation of the photophysically active $^3\text{MLCT}$ state to lower lying ^3MC and ^5MC states [32,33]. Nonetheless, since Fe is a bioessential metal, it is anticipated to have a reduced metal-induced cellular toxicity [34,35] in comparison to other metal-based complexes. Chakravarty and co-workers have already reported several Fe(III)-based complexes with a dipyrrido[3,2-d:2',3'-f]quinoxaline [35–37] or a dipicolylamine [34,38–45] moiety as effective PSs. As an impressive example, the Fe(III) complex **1** was prepared with a dipicolylamine ligand combined with an anthracenyl moiety, which is able to intercalate in the DNA, and a catechol ligand, which promotes an intense ligand-to-metal charge-transfer band in the near IR window (Figure 1). These complexes were shown to act as potent fluorophores and to have a nuclear uptake. Very importantly, they caused apoptotic cell death upon light irradiation [34]. Worthy of note, the same group also synthesized bimetallic Fe(III) complexes as PSs in view of DNA cleavage [46,47] and site specific protein cleavage [48]. Additionally, a recent publication by the same authors showed that the conjugation of a phototoxic Fe(III) complex to biotin allows for selective tumor delivery of the PDT agent [49]. In comparison to complexes with a +3 oxidation state, the studies of Fe complexes with a +2 oxidation state as a PS are scarce. Roelfes and co-workers have, for example, designed a series of Fe(II)-N4Py complexes (N4Py = *N,N*-bis(2-pyridylmethyl)-*N*-bis(2-pyridyl)methylamine) as effective PSs for DNA cleavage [50,51]. In addition, Fe(II)-terpyridine complexes with aromatic moieties, which were found to be localizing in the nucleus, showed a remarkable phototoxicity upon visible light irradiation while remaining only slightly cytotoxic in the dark [52]. A recent study has also demonstrated the use of pyridyldipyridophenazine substituted Fe(II) complexes as partial DNA intercalative binders. The complexes had phototoxicity upon visible light irradiation, in addition to a low dark toxicity [53].

Inspired from the works described above, we have decided to investigate the potential of Fe(II) polypyridyl complexes as chemotherapeutic agents and PDT PSs. For this, we capitalized on the work on Ru(II) polypyridine complexes and especially on the ones on 4,7-diphenyl-1,10-phenanthroline (bphen)-containing complexes [54–63]. With the work of Glazer and co-workers on the Ru(II) based complexes **2** and **3** in mind (Figure 1), we have designed the two analogous Fe(II) complexes (complexes **4** and **5**, Figure 2). We have also prepared an isomer of complex **5** (complex **6**, Figure 2). As demonstrated for the Ru(II) complexes, the substituents that were introduced in complexes **5** and **6** were able to drastically improve the water solubility of the complexes. At the same time,

this derivatization did not influence their photophysical properties [54,64]. Worthy of note, **4** has already been reported in the literature as a catalyst for the autoxidation of cumene and cyclohexane, demonstrating that this complex is able to interact with oxygen [65]. Herein, we present the synthesis, in-depth characterization, and biological evaluation of three Fe(II) complexes. As shown below, we were able to unveil a compound with cytotoxicity in the low micro molar range in the dark and some phototoxicity in RPE-1 and HeLa cells.

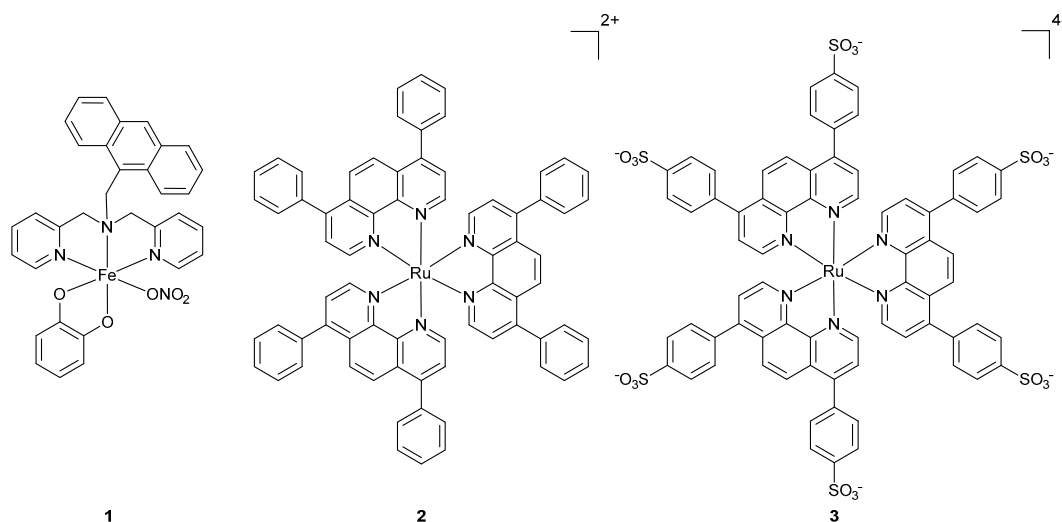


Figure 1. Chemical structures of a Fe(III) complex (**1**) investigated by Chakravarty and co-workers and Ru(II) bphen complexes (**2**, **3**) investigated by Glazer and co-workers as Photodynamic Therapy photosensitizers (PDT PSs).

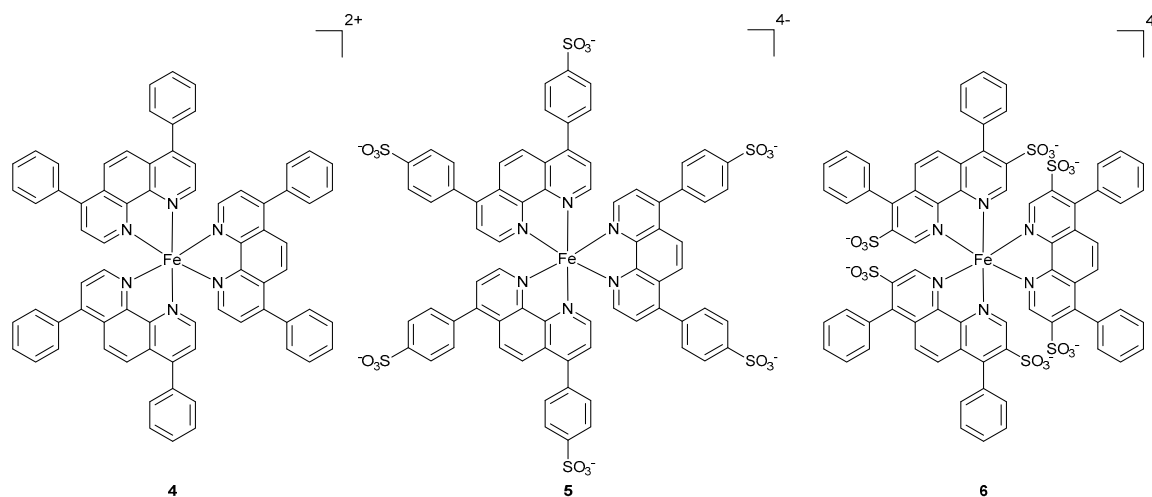


Figure 2. Chemical structures of the Fe(II) complexes investigated in this work. Complexes **4** was isolated as a PF₆ salt and the complexes **5** and **6** were isolated as Na salts.

2. Results and Discussion

2.1. Synthesis and Characterization

The complexes that were synthesized in this work are visualized in Figure 2. The synthesis of complex **4** has already been reported in the literature [65], contrary to those of complexes **5** and **6**. All of the complexes were synthesized by the complexation of bphen and its derivatives with FeCl₂·4H₂O. The identity of all complexes was confirmed by ¹H, ¹³C-NMR, and HRMS, and the purity by high performance liquid chromatography (HPLC) and elemental analysis (Figures S1–S9).

2.2. Photophysical Properties

After full chemical characterization, the photophysical properties of the prepared complexes were evaluated in view of potential applications as PDT PS. It is well established that the used wavelength in a PDT treatment has direct influence on the tissue light penetration depth and therefore the possibility to treat deep tumors. It is important to mention that there is no ideal PS for PDT due to the various applications of this technique as well as the different depth of a tumor. For deep seated tumors, absorption in the near-infrared region (NIR) is desired to have an increased light penetration depth. However, if the tumor is seated only on the surface, a deep penetration would be undesirable due to the possibility of damaging healthy underlying tissue. Worthy of note, PSs with very low extinction coefficients in the red region have already been shown to still be able to be activated [18,66,67]. Based on this, a major aim in the development of new (metal-based) PSs is a red shift of the absorption towards the therapeutic window (600 to 900 nm) [16]. Keeping this in mind, the absorption profile of all complexes (Figure 3) was measured in CH₃CN. Importantly, the compounds showed an absorption maximum at 530 nm for complex 4 and 535 nm for complexes 5 and 6 with an absorption tail in the photo-therapeutic window. For further investigation of the photophysical properties, the complexes were excited at 450 nm and the emission measured in CH₃CN. The luminescence of all complexes was found to be between 550 and 800 nm with an emission maximum at 610 nm for compound 4 and 620 nm for compounds 5 and 6 (Figures S10–S12). Worthy of note, the complexes were found to be only weakly emissive and the emission could only be measured at the detection limit of our apparatus with luminescence quantum yields <0.01% in CH₃CN. Additionally, the measurement of the excited state lifetimes in degassed and aerated CH₃CN was not possible due to a necessary minimal delay between excitation and detection with our apparatus, indicating that the compounds 4–6 have lifetimes <29 ns. These observations are fitting with other excited state studies, which confirm the low luminescence and very short lifetime of Fe complexes [68,69]. The comparison between all investigated complexes shows very similar absorption and emission properties, indicating that the additional sulfonic acid group in complex 5 and 6 does not significantly change the photophysical properties when compared to complex 4.

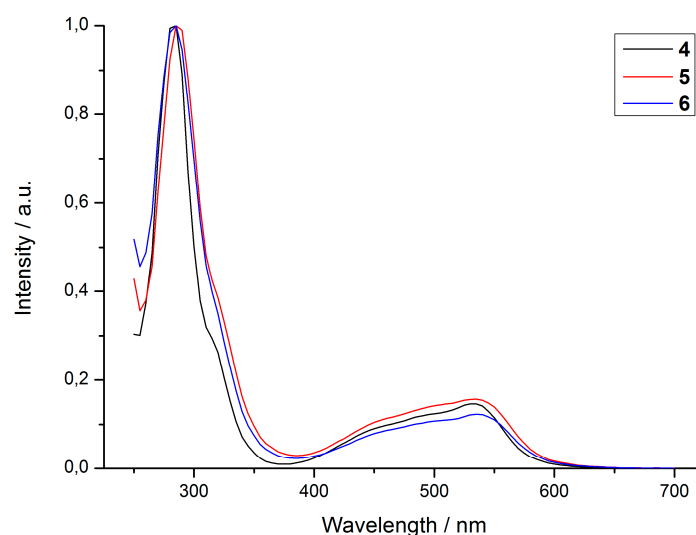


Figure 3. Normalized UV/Vis spectra of the complexes 4–6 in CH₃CN.

2.3. Singlet Oxygen Generation

Although there can be radicals involved, for most approved PSs, the formation of singlet oxygen (¹O₂) is the predominant species responsible for cell/bacteria death. Therefore, to assess the potential of our PSs, we have investigated their ability to produce ¹O₂ upon light irradiation. To quantitatively evaluate this, we used two methods: (1) a direct method by measurement of the phosphorescence of ¹O₂

and (2) an indirect method by measurement of the absorption changes of a reporter molecule [23,70]. The results (Table 1) show that complexes 4–6 are poorly producing $^1\text{O}_2$ with quantum yields from 2% to 4% in aerated CH_3CN and <1% in aerated PBS at the detection limit of our used system. These low values can be explained by the very short lifetime of the excited state. These short lifetimes are limiting the necessary energy transfer from the excited $^3\text{MLCT}$ state to molecular oxygen ($^3\text{O}_2$) to generate $^1\text{O}_2$.

Table 1. Singlet oxygen quantum yields ($\Phi(^1\text{O}_2)$) in CH_3CN and aqueous solution determined by a direct and an indirect method upon excitation at 450 nm. Average of three independent measurements ($\pm 10\%$).

Compounds	CH_3CN		D_2O		PBS	
	Direct Method	Indirect Method	Direct Method	Indirect Method	Direct Method	Indirect Method
4	n.d.	4%	n.d.	n.d.	n.d.	<1%
5	n.d.	2%	n.d.	n.d.	n.d.	<1%
6	n.d.	2%	n.d.	n.d.	n.d.	<1%

n.d. = not determinable.

2.4. Stability in Human Plasma

In PDT, the stability of the PS is crucial. Therefore, the stability of our complexes under physiological conditions, more specifically in human plasma, was investigated. For this purpose, all of the complexes were incubated in human plasma at 37 °C in the dark for 48 h. After extraction of the PS, its stability was analysed via high performance liquid chromatography (HPLC). As an internal reference, caffeine, which has already been shown to be stable under these conditions [71], was used. For analysis of the chromatograms (Figures S13–S15), the signal of the caffeine and of our complexes were integrated and the ratios before and after incubation in human plasma were compared. Since the ratio did not change significantly, we concluded that there is no decomposition in the tested time interval, confirming hence the stability of the compounds 4–6.

2.5. Photostability

Next to the stability in an biological environment, the stability of our compounds upon light exposure was investigated. The currently used PSs which are based on a tetrapyrrolic scaffold are known to undergo structural physical modifications (i.e., photobleaching) upon light irradiation [72,73]. To investigate this potential property of our metal complexes, they were exposed to a continuous LED irradiation for 120 min at 450 nm. The potential change of the absorption properties of the complexes were monitored by UV/Vis spectroscopy. As a positive control, $[\text{Ru}(\text{bipy})_3]\text{Cl}_2$ was used, whereas Protoporphyrin IX (PpIX) was employed as a negative control. The comparison of the temporal change of the investigated complexes 4–6 shows only a small decrease in the absorption profile for our three complexes (Figures S16–S20), in a similar fashion than $[\text{Ru}(\text{bipy})_3]\text{Cl}_2$. This indicates that light exposure has only a minimal effect on the stability of the compounds.

2.6. Distribution Coefficient

It is well known that the lipophilicity of a compound plays a crucial role in the extent of its cellular uptake and its cellular localisation [74,75]. Therefore, we investigated the lipophilicity of all synthesised compounds by using the “shake-flask” method. The complex was dissolved and repeatedly shaken between a PBS and octanol phase. After equilibration, the distribution between the organic and water phase was determined. As expected, due to the large lipophilic bphen ligands, compound 4 was found in the organic phase (Table 2). In comparison, complexes 5 and 6 with the additional sulfonic acid groups were found in the aqueous phase. Worthy of note, the Ru(II)-based analogous compounds were found to have very similar $\log P$ values [54], indicating that the metal ion does not significantly influence this value. Interestingly, compound 6 is more lipophilic than

compound **5**. This can be explained by the location of its sulfonic acid groups that are not decorated at the outside of the complex. They are therefore a bit shielded and they do not interact with water as much as complex **5**.

Table 2. Distribution coefficients of the compound **4–6** between Phosphate-Buffered Saline (PBS) and octanol. Average of three independent measurements.

Compound	log <i>P</i>
4	+1.7 ± 0.1
5	−2.2 ± 0.1
6	−1.9 ± 0.1

2.7. Cytotoxicity and Photocytotoxicity

After having assessed the (photo-)physical properties of our complexes, we have investigated the influence of our compounds on the cell viability in the dark and upon light irradiation. For this purpose, compounds **4–6** were incubated in non-cancerous retinal pigment epithelium (RPE-1) and human cervical carcinoma (HeLa) cells in the dark and upon irradiation at 480 and 540 nm. After 48 h, cell viability was assessed by exposing the cells to resazurin. An overview of the IC₅₀ values is presented in Table 3. Interestingly, complex **4** was found to be toxic in the dark in the low micromolar range, as the anticancer drug cisplatin. Disappointingly, light exposure had only a small effect on cell viability. These results were expected due to the poor generation of ¹O₂ upon light irradiation of our PSs. The phototoxic index (PI) is defined as the ratio between the IC₅₀ value in the dark and the IC₅₀ value upon light exposure. Complex **4** was found to have a PI value of 1.2 at 480 nm and 1.1 at 540 nm for RPE-1 cells and 1.3 at 480 nm and 1.4 at 540 nm in HeLa cells, respectively. These values are extremely low in comparison to established PDT PSs. In comparison, complexes **5** and **6** have no measurable cytotoxic effect in both the dark or upon light irradiation. Worthy of note, the dark cytotoxicities of **4** and **5** are in a very similar range than the Ru(II) analogous, which have been investigated by Glazer and co-workers in other cancer cell lines. This implies that the metal core is not primary responsible for the observed dark toxicity [54]. The comparison between the non-cancerous cell line RPE-1 and the human cervical carcinoma cell line HeLa shows no selectivity for cancer. Overall, this study demonstrates that a small structural change, like additional sulfonic acid groups at the outer sphere of the complex, completely changes the effect that these compounds have on the cells.

Table 3. IC₅₀ values in the dark and upon irradiation for the complexes **4–6** incubated in human cervical carcinoma (HeLa) and non-cancerous retinal pigment epithelium (RPE-1) cells. Average of three independent measurements.

	HeLa					RPE-1				
	IC ₅₀ /μM Dark	IC ₅₀ /μM 480 nm	PI	IC ₅₀ /μM 540 nm	PI	IC ₅₀ /μM Dark	IC ₅₀ /μM 480 nm	PI	IC ₅₀ /μM 540 nm	PI
4	9.3 ± 0.8	7.2 ± 0.6	1.3	6.6 ± 0.1	1.4	10.8 ± 1.0	9.3 ± 0.5	1.2	9.8 ± 0.5	1.1
5	>100	>100	n.d.	>100	n.d.	>100	>100	n.d.	>100	n.d.
6	>100	>100	n.d.	>100	n.d.	>100	>100	n.d.	>100	n.d.
PpIX	>100	2.5 ± 0.1	>40	2.1 ± 0.3	>48	>100	3.8 ± 0.1	>26	3.1 ± 0.1	>32
Cisplatin	10.5 ± 0.8	-	-	-	-	29.3 ± 1.4	-	-	-	-

n.d. = not determinable.

3. Materials and Methods

3.1. Instrumentation and Methods

¹H- and ¹³C-NMR spectra were recorded on a 400 MHz NMR spectrometer (Bruker France, Wissembourg, France). Chemical shifts (δ) are reported in parts per million (ppm) referenced to

tetramethylsilane (δ 0.00) ppm using the residual proton solvent peaks as internal standards. Coupling constants (J) are reported in Hertz (Hz) and the multiplicity is abbreviated, as follows: s (singlet), d (doublet), and m (multiplet). Electrospray Ionization-Mass Spectrometry (ESI-MS) experiments were carried out using a LTQ-Orbitrap XL from Thermo Scientific (Thermo Fisher Scientific, Courtaboeuf, France) and operated in positive ionization mode, with a spray voltage at 3.6 kV. No sheath and auxiliary gas was used. Applied voltages were 40 and 100 V for the ion transfer capillary and the tube lens, respectively. The ion transfer capillary was held at 275 °C. Detection was achieved in the Orbitrap with a resolution set to 100,000 (at m/z 400) and an m/z range between 150 and 2000 in profile mode. Spectrum was analyzed using the acquisition software XCalibur 2.1 (Thermo Fisher Scientific, Courtaboeuf, France). The automatic gain control (AGC) allowed for the accumulation of up to 2×10^5 ions for Fourier Transform Mass Spectrometry (FTMS) scans, maximum injection time was set to 300 ms and 1 μ s scan was acquired. 10 μ L was injected using a Thermo Finnigan Surveyor HPLC system (Thermo Fisher Scientific, Courtaboeuf, France) with a continuous infusion of methanol at 100 μ L \cdot min $^{-1}$. Elemental microanalyses were performed on a Thermo Flash 2000 elemental analyzer. For analytic HPLC, the following system has been used: 2 \times Agilent G1361 1260 Prep Pump system (Agilent Technologies, Massy, France) with Agilent G7115A 1260 DAD WR Detector equipped with an Agilent Pursuit XRs 5C18 (Analytic: 100 Å, C18 5 μ m 250 \times 4.6 mm, Preparative: 100 Å, C18 5 μ m 250 \times 300 mm) Column and an Agilent G1364B 1260-FC fraction collector. The solvents (HPLC grade) were millipore water (0.1% TFA, solvent A) and acetonitrile (0.1% TFA, solvent B). The following method was used: 0–3 min: isocratic 95% A (5% B); 3–17 min: linear gradient from 95% A (5% B) to 0% A (100% B); 17–23 min: isocratic 0% A (100% B).

3.2. Materials

All of the chemicals were obtained from commercial sources and were used without further purification. 4,7-Diphenyl-1,10-phenanthroline (98%) and Iron (II) chloride tetrahydrate (98%) were obtained from Alfa Aesar (Schiltigheim, France). Disodium-4,7-Diphenyl-1,10-phenanthroline-4',4''-disulfonic acid hydrate (98%) and Disodium-4,7-Diphenyl-1,10-phenanthroline-3,8-disulfonic acid hydrate (98%) were obtained from abcr GmbH (Karlsruhe, Germany). Dulbecco's Modified Eagles Medium (DMEM), Dulbecco's Modified Eagles Medium supplemented with nutrient mixture F-12 (DMEM/F-12), Fetal Bovine Serum (FBS), Gibco Penicillin-Streptomycin-Glutamine (Penstrep), Dulbecco's Phosphate-Buffered Saline (PBS) were purchased from Fisher Scientific (Illkirch, France), and Resazurin from ACROS Organics (Noisy le Grand, France).

3.3. Synthesis

Fe(4,7-Diphenyl-1,10-phenanthroline) $_3$ (PF $_6$) $_2$ (**1**): The synthesis of Fe(4,7-Diphenyl-1,10-phenanthroline) $_3$ (PF $_6$) $_2$ is already published [65]. However, in this work, another synthetic route was employed. 4,7-Diphenyl-1,10-phenanthroline (750 mg, 2.26 mmol) and FeCl $_2$ ·4H $_2$ O (128 mg, 0.65 mmol) were suspended in ethanol (50 mL) under nitrogen atmosphere and the mixture was refluxed for 16 h. After that, the solution was cooled down and undissolved residue was removed via filtration. To the obtained solution, an aqueous saturated solution of NH $_4$ PF $_6$ (5 mL) was added. The crude product, which precipitated as a PF $_6$ salt, was collected by centrifugation and washed with EtOH (20 mL), H $_2$ O (50 mL), and Et $_2$ O (50 mL). The crude product was dissolved in dichloromethane (100 mL) and washed with a 5% LiCl aqueous solution (3 \times 100 mL), brine (3 \times 100 mL) and H $_2$ O (3 \times 100 mL). The obtained solid was washed with pentane (100 mL) and dried under vacuum. 794 mg of **1** (0.59 mmol, 91%) were yielded as a dark red solid. 1 H-NMR (400 MHz, CD $_3$ CN, 298 K): 8.25 (s, 6H), 7.94 (d, 6H, J = 5.4 Hz), 7.67–7.60 (m, 30 H); 13 C-NMR (100 MHz, CD $_3$ CN, 298 K): 156.4, 151.3, 150.6, 136.5, 130.7, 130.7, 130.1, 129.5, 127.1, 126.9; ESI-HRMS: m/z 526.1640 [M] $^{2+}$ (calcd C $_{72}$ H $_{48}$ N $_6$ Fe, 526.1639); Elemental analysis for C $_{72}$ H $_{48}$ F $_{12}$ FeN $_6$ P $_2$ + C $_5$ H $_{12}$ (1427.12): Calcd.: C 65.33; H 4.28; N 5.94; Found: C 65.72; H 4.15; N 5.94.

Fe(4,7-Diphenyl-1,10-phenanthroline-4',4''-disulfonic acid)₃Na₆ (**2**): Disodium-4,7-Diphenyl-1,10-phenanthroline-4',4''-disulfonic acid (600 mg, 1.08 mmol) and FeCl₂·4H₂O (61 mg, 0.31 mmol) were suspended in ethanol (50 mL) under nitrogen atmosphere and the mixture was refluxed for 14 h. After that, the solution was cooled down and undissolved residue was removed via filtration. The crude product was dissolved in a H₂O/CH₃CN solution (50 mL) and fractionated precipitated by adding dropwise Et₂O. The obtained solid was washed with CHCl₃ (20 mL) and Et₂O (50 mL). The product was isolated after recrystallization from EtOH/Pentane. The obtained product was dried under vacuum. 211 mg of **2** (0.13 mmol, 42%) were yielded as a dark solid. ¹H-NMR (400 MHz, CD₃OD, 298 K): 8.34 (s, 6H), 8.12–8.03 (m, 18H), 7.80–7.70 (m, 18H); ¹³C-NMR (100 MHz, CD₃OD, 298 K): 156.8, 151.8, 150.6, 147.6, 137.0, 132.7, 130.0, 128.4, 127.8, 127.7; ESI-HRMS *m/z* 381.5065 [M]⁴⁻ (calcd C₇₂H₄₂N₆O₁₈S₆Fe, 381.5063); Elemental analysis for C₇₂H₄₂FeN₆Na₆O₁₈S₆ (1665.30): Calcd.: C 51.93; H 2.54; N 5.05; Found: C 51.86; H 2.50; N 4.92.

Fe(4,7-Diphenyl-1,10-phenanthroline-3,8-disulfonic acid)₃Na₆ (**3**): Disodium-4,7-Diphenyl-1,10-phenanthroline-3,8-disulfonic acid (696 mg, 1.30 mmol) and FeCl₂·4H₂O (81 mg, 0.41 mmol) were suspended in ethanol (50 mL) under nitrogen atmosphere and the mixture was refluxed for 16 h. After that, the solution was cooled down and undissolved residue was removed via filtration. The crude product was dissolved in a H₂O/CH₃CN solution (50 mL) and fractionated precipitated by adding dropwise Et₂O. The product was isolated after recrystallization from EtOH/Pentane. The obtained product was dried under vacuum. 178 mg of **3** (0.11 mmol, 27%) were yielded as a dark solid. ¹H-NMR (400 MHz, CD₃OD, 298 K): 8.35 (s, 6H), 8.12–8.01 (m, 18H), 7.81–7.65 (m, 18H); ¹³C-NMR (100 MHz, CD₃OD, 298 K): 156.8, 151.8, 150.6, 147.6, 137.1, 132.7, 130.0, 128.4, 127.7, 125.4. ESI-HRMS *m/z* 381.5063 [M]⁴⁻ (calcd C₇₂H₄₂N₆O₁₈S₆Fe, 381.5063); Elemental analysis for C₇₂H₄₂FeN₆Na₆O₁₈S₆ (1665.30): Calcd.: C 51.93; H 2.54; N 5.05; Found: C 51.80; H 2.47; N 4.93.

3.4. Spectroscopic Measurements

The absorption of the samples has been measured with a SpectraMax M2 Spectrometer (Molecular Devices, San Jose, CA, USA). The emission was measured by irradiation of the sample in fluorescence quartz cuvettes (width 1 cm) using a NT342B Nd-YAG pumped optical parametric oscillator (Ekspla, Vilnius, Lithuania) at 450 nm. Luminescence was focused and collected at a right angle to the excitation pathway and it was directed to a Princeton Instruments Acton SP-2300i monochromator. As a detector a PI-Max 4 CCD camera (Princeton Instruments, Trenton, NJ, USA) has been used.

3.5. Luminescence Quantum Yield Measurements

For the determination of the luminescence quantum yield, the samples were prepared in a CH₃CN solution with an absorbance of 0.1 at 450 nm. This solution was irradiated in fluorescence quartz cuvettes (width 1 cm) using a NT342B Nd-YAG pumped optical parametric oscillator (Ekspla, Vilnius, Lithuania) at 450 nm. The emission signal was focused and collected at a right angle to the excitation pathway and it was directed to a Princeton Instruments Acton SP-2300i monochromator. As a detector, a PI-Max 4 CCD camera (Princeton Instruments, Trenton, NJ, USA) has been used. The luminescence quantum yields were determined by comparison with the reference [Ru(bipy)₃]Cl₂ in CH₃CN ($\Phi_{em} = 5.9\%$) [76] applying the following formula:

$$\Phi_{em, sample} = \Phi_{em, reference} \times (F_{reference}/F_{sample}) \times (I_{sample}/I_{reference}) \times (n_{sample}/n_{reference})^2$$

$$F = 1 - 10^{-A}$$

Φ_{em} = luminescence quantum yield, F = fraction of light absorbed, I = integrated emission intensities, n = refractive index, A = absorbance of the sample at irradiation wavelength.

3.6. Lifetime Measurements

For the determination of the lifetimes, the samples were prepared in an air saturated and in a degassed CH₃CN solution with an absorbance of 0.1 at 355 nm. This solution was irradiated in fluorescence quartz cuvettes (width 1 cm) using a NT342B Nd-YAG pumped optical parametric oscillator (Ekspla, Vilnius, Lithuania) at 450 nm. The emission signal was focused and collected at right angle to the excitation pathway and directed to a Princeton Instruments Acton SP-2300i monochromator. As a detector, a R928 photomultiplier tube (Hamamatsu, Hamamatsu, Japan) has been used.

3.6.1. Singlet Oxygen Measurements - Direct evaluation

The samples were prepared in an air saturated CH₃CN or D₂O solution with an absorbance of 0.2 at 450 nm. This solution was irradiated in fluorescence quartz cuvettes (width 1 cm) using a mounted M450LP1 LED (Thorlabs, Dachau, Germany), whose irradiation, centered at 450 nm, has been focused with aspheric condenser lenses. The intensity of the irradiation has been varied using a T-Cube LED Driver (Thorlabs, Dachau, Germany) and measured with an optical power and energy meter. The emission signal was focused and collected at right angle to the excitation pathway and directed to a Princeton Instruments Acton SP-2300i monochromator. A longpass glass filter was placed in front of the monochromator entrance slit to cut off light at wavelengths shorter than 850 nm. As a detector an EO-817L IR-sensitive liquid nitrogen cooled germanium diode detector (North Coast Scientific Corp., Santa Rosa, CA, USA) has been used. The singlet oxygen luminescence at 1270 nm was measured by recording spectra from 1100 to 1400 nm. For the data analysis, the singlet oxygen luminescence peaks at different irradiation intensities were integrated. The resulting areas were plotted against the percentage of the irradiation intensity and the slope of the linear regression was calculated. The absorbance of the sample was corrected with an absorbance correction factor. As reference for the measurement in an CH₃CN solution phenalene ($\Phi_{\text{phenalene}} = 95\%$) [77] and for the measurement in a D₂O solution [Ru(bipy)₃]Cl₂ ($\Phi_{\text{Ru(bipy)3Cl2}} = 22\%$) [78] was used and the singlet oxygen quantum yields were calculated while using the following formula:

$$\Phi_{\text{sample}} = \Phi_{\text{reference}} \times (S_{\text{sample}}/S_{\text{reference}}) \times (I_{\text{reference}}/I_{\text{sample}})$$

$$I = I_0 * (1 - 10^{-A})$$

Φ = singlet oxygen quantum yield, S = slope of the linear regression of the plot of the areas of the singlet oxygen luminescence peaks against the irradiation intensity, I = absorbance correction factor, I_0 = light intensity of the irradiation source, and A = absorbance of the sample at irradiation wavelength.

3.6.2. Singlet Oxygen Measurements - Indirect evaluation

For the measurement in CH₃CN: The samples were prepared in an air-saturated CH₃CN solution containing the complex with an absorbance of 0.2 at the irradiation wavelength, *N,N*-dimethyl-4-nitrosoaniline aniline (RNO, 24 μ M) and imidazole (12 mM). For the measurement in PBS buffer: The samples were prepared in an air-saturated PBS solution containing the complex with an absorbance of 0.1 at the irradiation wavelength, *N,N*-dimethyl-4-nitrosoaniline aniline (RNO, 20 μ M), and histidine (10 mM). The samples were irradiated on 96 well plates with an Atlas Photonics LUMOS BIO irradiator (Atlas Photonics, Fribourg, Switzerland) for different times. The absorbance of the samples was measured during these time intervals with a SpectraMax M2 Microplate Reader (Molecular Devices, San Jose, CA, USA). The difference in absorbance ($A_0 - A$) at 420 nm for the CH₃CN solution or at 440 nm a PBS buffer solution was calculated and plotted against the irradiation times. From the plot, the slope of the linear regression was calculated as well as the absorbance correction factor determined. The singlet oxygen quantum yields were calculated using the same formulas as used for the direct evaluation.

3.7. Stability in Human Plasma

The stability of the complexes was evaluated with caffeine as an internal standard, which has already been shown to be suitable for these experiments [71]. The pooled human plasma was obtained from Biowest and caffeine from TCI Chemicals. Stock solutions of the compounds (20 μM) and caffeine (40 μM) were prepared in DMSO. One aliquot of the solutions was added to 975 μL of human plasma to a total volume of 1000 μL . Final concentrations of the compounds of 0.25 μM and caffeine of 0.5 μM were achieved. The resulting solution was incubated for 48 h at 37 $^{\circ}\text{C}$ with continuous gentle shaking (ca. 300 rpm). The reaction was stopped after the incubation time by the addition of 3 mL of methanol. The mixture was centrifuged for 60 min at 3000 rpm at 4 $^{\circ}\text{C}$. The methanolic solution was filtered through a 0.2 μm membrane filter. The solvent was evaporated under reduced pressure and the residue was dissolved in 1:1 (*v/v*) $\text{CH}_3\text{CN}/\text{H}_2\text{O}$ 0.1% TFA solution. The solution was filtered through a 0.2 μm membrane filter and analyzed using a HPLC System (Agilent Technologies, Massy, France).

3.8. Photostability

The samples were prepared in an air saturated CH_3CN solution with an absorbance of about 0.5 at 450 nm. To measure the photostability, the samples were irradiated at 450 nm in 96 well plates with an Atlas Photonics LUMOS BIO irradiator (Atlas Photonics, Fribourg, Switzerland) during time intervals from 0 to 120 min. The absorbance spectrum from 350 to 700 nm was recorded with a SpectraMax M2 Microplate Reader (Molecular Devices, San Jose, CA, USA) after each time interval and then compared. As a positive control $[\text{Ru}(\text{bipy})_3]\text{Cl}_2$ and as a negative control Protoporphyrin IX has been used.

3.9. Distribution Coefficient

The lipophilicity of a compound was determined by measuring its distribution coefficient between the PBS and Octanol phase by using the “shake-flask” method. For this technique, the used phases were previously saturated in each other. The compound was dissolved in the phase (A) with its major presence with an absorbance of about 0.5 at 450 nm. This solution was then mixed with an equal volume of the other phase (B) at 80 rpm for 8 h with an Invitrogen sample mixer and then equilibrated overnight. The phase A was then carefully separated from phase B. The amount of the compound before and after the sample mixing was determined by UV/Vis spectroscopy at 450 nm using a SpectraMax M2 Microplate Reader (Molecular Devices, San Jose, CA, USA). The evaluation of the complexes was repeated three times and the ratio between the organic and aqueous phase calculated.

3.10. Cell Culture

Human cervical carcinoma (HeLa) cells were cultured using DMEM media and retinal pigment epithelium (RPE-1) cells using DMEM/F-12 with addition of 10% FBS and 1% penstrep. The cells were cultivated and maintained at 37 $^{\circ}\text{C}$ in a cell culture incubator at 37 $^{\circ}\text{C}$ with 5% CO_2 atmosphere. Before an experiment, the cells were passaged three times.

3.11. Cytotoxicity and Photocytotoxicity

The cytotoxicity of the compounds was accessed by measuring the cell viability using a fluorometric resazurin assay. The cultivated cells were seeded in triplicates in 96 well plates with a density of 4000 cells per well in 100 μL of media. After 24 h, the medium was removed and the cells were treated with increasing concentrations of the compound diluted in cell media achieving a total volume of 200 μL . The cells were incubated with the compound for 4 h. After this time, the media was removed and replaced with 200 μL of fresh medium. For the phototoxicity studies, the cells were exposed to light with an Atlas Photonics LUMOS BIO irradiator (Atlas Photonics, Fribourg, Switzerland). Each well was constantly illuminated with either a 480 nm or 510 nm irradiation. During this time, the temperature was maintained constantly at 37 $^{\circ}\text{C}$. The cells were grown in the incubator for an additional 44 h. For the determination of the dark cytotoxicity, the cells were not irradiated and after the medium exchange

directly incubated for 44 h. After this time, the medium was replaced with fresh medium containing resazurin with a final concentration of 0.2 mg/mL. After 4 h incubation, the amount of the fluorescent product resorufin was determined upon excitation at 540 nm and measurement of its emission at 590 nm using a SpectraMax M2 Microplate Reader (Molecular Devices, San Jose, CA, USA). The obtained data was analyzed with the GraphPad Prism software.

4. Conclusions

In this work, we report on the characterization and biological properties of three Fe(II) complexes containing different derivatives of 4,7-diphenyl-1,10-phenanthroline (bphen) (complexes 4–6). The complexes were found to absorb strongly in the red region, which is a desired and important requirement for PDT treatment of deep cancers. Stability studies in human plasma as well as photostability studies showed that the investigated complexes are stable in physiological conditions and importantly do not have a photobleaching effect as some of the currently approved PDT PSs. Photophysical studies of these compounds revealed that they are weakly luminescent, have a very short lived excited state, and are poorly producing singlet oxygen. Interestingly, the addition of sulfonic acid groups to the bphen ligand to give complexes 5 and 6 do not significantly change these properties. However, as expected, these groups are able to strongly increase the water solubility of the complexes. Complexes 5 and 6 were shown to have no cytotoxic effect in the dark as well as upon light exposure contrary to compound 4 that had a dark toxicity in the low micromolar range. Light exposure was shown to have only a small effect on cell viability. We assume that this is due to the poor photophysical properties (i.e., short luminescent lifetimes and poor $^1\text{O}_2$ production) of the complexes. We are currently investigating other options to prepare Fe(II) complexes with longer luminescent lifetimes, which will be more appropriate for PDT applications.

Supplementary Materials: The following are available online at <http://www.mdpi.com/2304-6740/7/1/4/s1>, Figure S1. ^1H -NMR spectrum of 4 in CD_3CN , 400 MHz, Figure S2. ^{13}C -NMR spectrum of 4 in CD_3CN , 100 MHz, Figure S3. ESI-HRMS spectrum of 4 (positive detection mode), Figure S4. ^1H -NMR spectrum of 5 in CD_3OD , 400 MHz, Figure S5. ^{13}C -NMR spectrum of 5 in CD_3OD , 100 MHz, Figure S6. ESI-HRMS spectrum of 5 (negative detection mode), Figure S7. ^1H -NMR spectrum of 6 in CD_3OD , 400 MHz, Figure S8. ^{13}C -NMR spectrum of 6 in CD_3OD , 100 MHz, Figure S9. ESI-HRMS spectrum of 6 (negative detection mode), Figure S10. Normalised Emission Spectrum of 4 in CH_3CN , Figure S11. Normalised Emission Spectrum of 5 in CH_3CN , Figure S12. Normalised Emission Spectrum of 6 in CH_3CN , Figure S13. HPLC chromatogram of Caffeine (internal standard) and 4 after 0 and 48 h incubation in human pooled plasma, Figure S14. HPLC chromatogram of Caffeine (internal standard) and 5 after 0 and 48 h incubation in human pooled plasma, Figure S15. HPLC chromatogram of Caffeine (internal standard) and 6 after 0 and 48 h incubation in human pooled plasma, Figure S16. Temporal change of the UV/Vis spectra of $[\text{Ru}(\text{bipy})_3]\text{Cl}_2$ by irradiation at 450 nm in CH_3CN , Figure S17. Temporal change of the UV/Vis spectra of 4 by irradiation at 450 nm in CH_3CN , Figure S18. Temporal change of the UV/Vis spectra of 5 by irradiation at 450 nm in CH_3CN , Figure S19. Temporal change of the UV/Vis spectra of 6 by irradiation at 450 nm in CH_3CN , Figure S20. Temporal change of the UV/Vis spectra of PpIX by irradiation at 450 nm in CH_3CN .

Author Contributions: J.K. conceived, designed, performed the experiments and analyzed the data. The project was conceived, designed and supervised by P.G. and G.G.

Funding: This work was financially supported by an ERC Consolidator Grant PhotoMedMet to G.G. (GA 681679) and has received support under the program “Investissements d’Avenir” launched by the French Government and implemented by the ANR with the reference ANR-10-IDEX-0001-02 PSL (G.G.).

Acknowledgments: We thank Oliver Wenger for helpful discussions.

Conflicts of Interest: The authors declare no conflict of interest.

References

1. Jemal, A.; Bray, F.; Center, M.M.; Ferlay, J.; Ward, E.; Forman, D. Global cancer statistics. *CA Cancer J. Clin.* **2011**, *61*, 69–90. [[CrossRef](#)] [[PubMed](#)]
2. Urruticoechea, A.; Alemany, R.; Balart, J.; Villanueva, A.; Vinals, F.; Capella, G. Recent advances in cancer therapy: An overview. *Curr. Pharm. Des.* **2010**, *16*, 3–10. [[CrossRef](#)] [[PubMed](#)]
3. Gasser, G.; Metzler-Nolte, N. The potential of organometallic complexes in medicinal chemistry. *Curr. Opin. Chem. Biol.* **2012**, *16*, 84–91. [[CrossRef](#)] [[PubMed](#)]

4. Joshi, T.; Pierroz, V.; Mari, C.; Gemperle, L.; Ferrari, S.; Gasser, G. A bis (dipyridophenazine)(2-(2-pyridyl) pyrimidine-4-carboxylic acid) ruthenium(II) complex with anticancer action upon photodeprotection. *Angew. Chem. Int. Ed.* **2014**, *53*, 2960–2963. [[CrossRef](#)] [[PubMed](#)]
5. Gasser, G.; Ott, I.; Metzler-Nolte, N. Organometallic anticancer compounds. *J. Med. Chem.* **2010**, *54*, 3–25. [[CrossRef](#)] [[PubMed](#)]
6. Notaro, A.; Gasser, G. Monomeric and dimeric coordinatively saturated and substitutionally inert Ru(II) polypyridyl complexes as anticancer drug candidates. *Chem. Soc. Rev.* **2017**, *46*, 7317–7337. [[CrossRef](#)] [[PubMed](#)]
7. Zeng, L.; Gupta, P.; Chen, Y.; Wang, E.; Ji, L.; Chao, H.; Chen, Z.-S. The development of anticancer ruthenium(II) complexes: From single molecule compounds to nanomaterials. *Chem. Soc. Rev.* **2017**, *46*, 5771–5804. [[CrossRef](#)]
8. Johnstone, T.C.; Suntharalingam, K.; Lippard, S.J. The next generation of platinum drugs: Targeted Pt(II) agents, nanoparticle delivery, and Pt (IV) prodrugs. *Chem. Rev.* **2016**, *116*, 3436–3486. [[CrossRef](#)]
9. Süss-Fink, G. Arene ruthenium complexes as anticancer agents. *Dalton Trans.* **2010**, *39*, 1673–1688. [[CrossRef](#)]
10. Allardyce, C.S.; Dyson, P.J. Ruthenium in medicine: Current clinical uses and future prospects. *Platinum Met. Rev.* **2001**, *45*, 62–69.
11. Adhireksan, Z.; Davey, G.E.; Campomanes, P.; Groessel, M.; Clavel, C.M.; Yu, H.; Nazarov, A.A.; Yeo, C.H.F.; Ang, W.H.; Dröge, P.; et al. Ligand substitutions between ruthenium–cymene compounds can control protein versus DNA targeting and anticancer activity. *Nat. Commun.* **2014**, *5*, 3462. [[CrossRef](#)] [[PubMed](#)]
12. Brabec, V.; Pracharova, J.; Stepankova, J.; Sadler, P.J.; Kasparkova, J. Photo-induced DNA cleavage and cytotoxicity of a ruthenium(II) arene anticancer complex. *J. Inorg. Biochem.* **2016**, *160*, 149–155. [[CrossRef](#)] [[PubMed](#)]
13. Bruijninx, P.C.; Sadler, P.J. New trends for metal complexes with anticancer activity. *Curr. Opin. Chem. Biol.* **2008**, *12*, 197–206. [[CrossRef](#)] [[PubMed](#)]
14. Plaetzer, K.; Krammer, B.; Berlanda, J.; Berr, F.; Kiesslich, T. Photophysics and photochemistry of photodynamic therapy: Fundamental aspects. *Lasers Med. Sci.* **2009**, *24*, 259–268. [[CrossRef](#)] [[PubMed](#)]
15. O'Connor, A.E.; Gallagher, W.M.; Byrne, A.T. Porphyrin and nonporphyrin photosensitizers in oncology: Preclinical and clinical advances in photodynamic therapy. *Photochem. Photobiol.* **2009**, *85*, 1053–1074. [[CrossRef](#)]
16. Heinemann, F.; Karges, J.; Gasser, G. Critical overview of the use of Ru(II) polypyridyl complexes as photosensitizers in one-photon and two-photon photodynamic therapy. *Acc. Chem. Res.* **2017**, *50*, 2727–2736. [[CrossRef](#)]
17. Mari, C.; Pierroz, V.; Ferrari, S.; Gasser, G. Combination of Ru(II) complexes and light: New frontiers in cancer therapy. *Chem. Sci.* **2015**, *6*, 2660–2686. [[CrossRef](#)]
18. Monroe, S.; Colón, K.L.; Yin, H.; Roque, J., III; Konda, P.; Gujar, S.; Thummel, R.P.; Lilge, L.; Cameron, C.G.; McFarland, S.A. Transition metal complexes and photodynamic therapy from a tumor-centered approach: Challenges, opportunities, and highlights from the development of TLD1433. *Chem. Rev.* **2018**. [[CrossRef](#)]
19. McKenzie, L.K.; Bryant, H.E.; Weinstein, J.A. Transition metal complexes as photosensitizers in one- and two-photon photodynamic therapy. *Coord. Chem. Rev.* **2018**, *379*, 2–29. [[CrossRef](#)]
20. Mari, C.; Pierroz, V.; Rubbiani, R.; Patra, M.; Hess, J.; Spingler, B.; Oehninger, L.; Schur, J.; Ott, I.; Salassa, L. DNA intercalating Ru^{II} polypyridyl complexes as effective photosensitizers in photodynamic therapy. *Chem. Eur. J.* **2014**, *20*, 14421–14436. [[CrossRef](#)]
21. Mari, C.; Pierroz, V.; Leonidova, A.; Ferrari, S.; Gasser, G. Towards selective light-activated Ru^{II}-based prodrug candidates. *Eur. J. Inorg. Chem.* **2015**, *2015*, 3879–3891. [[CrossRef](#)]
22. Huang, H.; Yu, B.; Zhang, P.; Huang, J.; Chen, Y.; Gasser, G.; Ji, L.; Chao, H. Highly charged ruthenium(II) polypyridyl complexes as lysosome-localized photosensitizers for two-photon photodynamic therapy. *Angew. Chem.* **2015**, *127*, 14255–14258. [[CrossRef](#)]
23. Ellahioui, Y.; Patra, M.; Mari, C.; Kaabi, R.; Karges, J.; Gasser, G.; Gómez-Ruiz, S. Mesoporous silica nanoparticles functionalised with a photoactive ruthenium(II) complex: Exploring the formulation of a metal-based photodynamic therapy photosensitizer. *Dalton Trans.* **2019**. [[CrossRef](#)] [[PubMed](#)]
24. Lazic, S.; Kaspler, P.; Shi, G.; Monroe, S.; Sainuddin, T.; Forward, S.; Kasimova, K.; Hennigar, R.; Mandel, A.; McFarland, S. Novel osmium-based coordination complexes as photosensitizers for panchromatic photodynamic therapy. *Photochem. Photobiol.* **2017**, *93*, 1248–1258. [[CrossRef](#)] [[PubMed](#)]

25. Sun, Y.; Joyce, L.E.; Dickson, N.M.; Turro, C. DNA photocleavage by an osmium(II) complex in the PDT window. *Chem. Commun.* **2010**, *46*, 6759–6761. [[CrossRef](#)] [[PubMed](#)]
26. Holder, A.A.; Zigler, D.F.; Tarrago-Trani, M.T.; Storrie, B.; Brewer, K.J. Photobiological impact of $[(\text{bpy})_2\text{Ru}(\text{dpp})_2\text{RhCl}_2]\text{Cl}_5$ and $[(\text{bpy})_2\text{Os}(\text{dpp})_2\text{RhCl}_2]\text{Cl}_5$ [bpy = 2,2'-bipyridine; dpp = 2,3-bis(2-pyridyl)pyrazine] on vero cells. *Inorg. Chem.* **2007**, *46*, 4760–4762. [[CrossRef](#)] [[PubMed](#)]
27. Swavey, S.; Brewer, K.J. Visible light induced photocleavage of DNA by a mixed-metal supramolecular complex: $[(\text{bpy})_2\text{Ru}(\text{dpp})_2\text{RhCl}_2]^{5+}$. *Inorg. Chem.* **2002**, *41*, 6196–6198. [[CrossRef](#)]
28. Zamora, A.; Viguera, G.; Rodríguez, V.; Santana, M.D.; Ruiz, J. Cyclometalated iridium(III) luminescent complexes in therapy and phototherapy. *Coord. Chem. Rev.* **2018**, *360*, 34–76. [[CrossRef](#)]
29. McKenzie, L.K.; Sazanovich, I.V.; Baggaley, E.; Bonneau, M.; Guerschais, V.; Williams, J.A.; Weinstein, J.A.; Bryant, H.E. Metal complexes for two-photon photodynamic therapy: A cyclometalated iridium complex induces two-photon photosensitization of cancer cells under near-IR light. *Chem. Eur. J.* **2017**, *23*, 234–238. [[CrossRef](#)]
30. Huang, H.; Banerjee, S.; Sadler, P.J. Recent advances in the design of targeted iridium(III) photosensitizers for photodynamic therapy. *ChemBioChem* **2018**, *19*, 1574–1589. [[CrossRef](#)]
31. Basu, U.; Otto, S.; Heinze, K.; Gasser, G. Biological evaluation of the NIR-emissive ruby analogue $[\text{Cr}(\text{ddpd})_2][\text{BF}_4]_3$ as a photodynamic therapy photosensitizer. *Eur. J. Inorg. Chem.* **2018**. [[CrossRef](#)]
32. Mengel, A.K.; Bissinger, C.; Dorn, M.; Back, O.; Förster, C.; Heinze, K. Boosting Vis/NIR charge-transfer absorptions of iron(II) complexes by N-alkylation and N-deprotonation in the ligand backbone. *Chem. Eur. J.* **2017**, *23*, 7920–7931. [[CrossRef](#)]
33. Zhang, W.; Alonso-Mori, R.; Bergmann, U.; Bressler, C.; Chollet, M.; Galler, A.; Gawelda, W.; Hadt, R.G.; Hartsock, R.W.; Kroll, T.; et al. Tracking excited-state charge and spin dynamics in iron coordination complexes. *Nature* **2014**, *509*, 345. [[CrossRef](#)]
34. Basu, U.; Khan, I.; Hussain, A.; Kondaiah, P.; Chakravarty, A.R. Photodynamic effect in near-IR light by a photocytotoxic iron(III) cellular imaging agent. *Angew. Chem. Int. Ed.* **2012**, *51*, 2658–2661. [[CrossRef](#)]
35. Roy, M.; Saha, S.; Patra, A.K.; Nethaji, M.; Chakravarty, A.R. Ternary iron(III) complex showing photocleavage of DNA in the photodynamic therapy window. *Inorg. Chem.* **2007**, *46*, 4368–4370. [[CrossRef](#)]
36. Saha, S.; Majumdar, R.; Roy, M.; Dighe, R.R.; Chakravarty, A.R. An iron complex of dipyrrophenazine as a potent photocytotoxic agent in visible light. *Inorg. Chem.* **2009**, *48*, 2652–2663. [[CrossRef](#)]
37. Saha, S.; Mallick, D.; Majumdar, R.; Roy, M.; Dighe, R.R.; Jemmis, E.D.; Chakravarty, A.R. Structure–activity relationship of photocytotoxic iron(III) complexes of modified dipyrrophenazine ligands. *Inorg. Chem.* **2011**, *50*, 2975–2987. [[CrossRef](#)]
38. Basu, U.; Pant, I.; Kondaiah, P.; Chakravarty, A.R. Mitochondria-targeting iron(III) catecholates for photoactivated anticancer activity under red light. *Eur. J. Inorg. Chem.* **2016**, *2016*, 1002–1012. [[CrossRef](#)]
39. Basu, U.; Pant, I.; Khan, I.; Hussain, A.; Kondaiah, P.; Chakravarty, A.R. Iron(III) catecholates for cellular imaging and photocytotoxicity in red light. *Chem. Asian J.* **2014**, *9*, 2494–2504. [[CrossRef](#)]
40. Sahoo, S.; Podder, S.; Garai, A.; Majumdar, S.; Mukherjee, N.; Basu, U.; Nandi, D.; Chakravarty, A.R. Iron(III) complexes of vitamin b6 schiff base with boron-dipyrromethene pendants for lysosome-selective photocytotoxicity. *Eur. J. Inorg. Chem.* **2018**, *2018*, 1522–1532. [[CrossRef](#)]
41. Garai, A.; Pant, I.; Bhattacharyya, A.; Kondaiah, P.; Chakravarty, A.R. Mitochondria-targeted anticancer activity of bodipy-appended iron(III) catecholates in red light. *ChemistrySelect* **2017**, *2*, 11686–11692. [[CrossRef](#)]
42. Basu, U.; Khan, I.; Hussain, A.; Gole, B.; Kondaiah, P.; Chakravarty, A.R. Carbohydrate-appended tumor targeting iron(III) complexes showing photocytotoxicity in red light. *Inorg. Chem.* **2014**, *53*, 2152–2162. [[CrossRef](#)]
43. Basu, U.; Pant, I.; Hussain, A.; Kondaiah, P.; Chakravarty, A.R. Iron(III) complexes of a pyridoxal schiff base for enhanced cellular uptake with selectivity and remarkable photocytotoxicity. *Inorg. Chem.* **2015**, *54*, 3748–3758. [[CrossRef](#)]
44. Garai, A.; Basu, U.; Khan, I.; Pant, I.; Hussain, A.; Kondaiah, P.; Chakravarty, A.R. Iron(III) benzhydroxamates of dipicolylamines for photocytotoxicity in red light and cellular imaging. *Polyhedron* **2014**, *73*, 124–132. [[CrossRef](#)]
45. Garai, A.; Pant, I.; Kondaiah, P.; Chakravarty, A.R. Iron(III) salicylates of dipicolylamine bases showing photo-induced anticancer activity and cytosolic localization. *Polyhedron* **2015**, *102*, 668–676. [[CrossRef](#)]

46. Roy, M.; Santhanagopal, R.; Chakravarty, A.R. DNA binding and oxidative DNA cleavage activity of (μ -oxo) diiron(III) complexes in visible light. *Dalton Trans.* **2009**, *6*, 1024–1033. [[CrossRef](#)]
47. Roy, M.; Bhowmick, T.; Ramakumar, S.; Nethaji, M.; Chakravarty, A.R. Double-strand DNA cleavage from photodecarboxylation of (μ -oxo) diiron(III) L-histidine complex in visible light. *Dalton Trans.* **2008**, *27*, 3542–3545. [[CrossRef](#)]
48. Roy, M.; Bhowmick, T.; Santhanagopal, R.; Ramakumar, S.; Chakravarty, A.R. Photo-induced double-strand DNA and site-specific protein cleavage activity of L-histidine (μ -oxo) diiron(III) complexes of heterocyclic bases. *Dalton Trans.* **2009**, *24*, 4671–4682. [[CrossRef](#)]
49. Saha, S.; Majumdar, R.; Hussain, A.; Dighe, R.R.; Chakravarty, A.R. Biotin-conjugated tumour-targeting photocytotoxic iron(III) complexes. *Phil. Trans. R. Soc. A* **2013**, *371*, 20120190. [[CrossRef](#)]
50. Li, Q.; van den Berg, T.A.; Feringa, B.L.; Roelfes, G. Mononuclear Fe(II)-N4Py complexes in oxidative DNA cleavage: Structure, activity and mechanism. *Dalton Trans.* **2010**, *39*, 8012–8021. [[CrossRef](#)]
51. Li, Q.; Browne, W.R.; Roelfes, G. DNA cleavage activity of Fe(II) N4Py under photo irradiation in the presence of 1,8-naphthalimide and 9-aminoacridine: Unexpected effects of reactive oxygen species scavengers. *Inorg. Chem.* **2011**, *50*, 8318–8325. [[CrossRef](#)]
52. Basu, U.; Khan, I.; Koley, D.; Saha, S.; Kondaiiah, P.; Chakravarty, A.R. Nuclear targeting terpyridine iron(II) complexes for cellular imaging and remarkable photocytotoxicity. *J. Inorg. Biochem.* **2012**, *116*, 77–87. [[CrossRef](#)]
53. Garai, A.; Basu, U.; Pant, I.; Kondaiiah, P.; Chakravarty, A.R. Polypyridyl iron(II) complexes showing remarkable photocytotoxicity in visible light. *J. Chem. Sci.* **2015**, *127*, 609–618. [[CrossRef](#)]
54. Dickerson, M.; Sun, Y.; Howerton, B.; Glazer, E.C. Modifying charge and hydrophilicity of simple Ru(II) polypyridyl complexes radically alters biological activities: Old complexes, surprising new tricks. *Inorg. Chem.* **2014**, *53*, 10370–10377. [[CrossRef](#)]
55. Castellano, F.N.; Lakowicz, J.R. A water-soluble luminescence oxygen sensor. *Photochem. Photobiol.* **1998**, *67*, 179–183. [[CrossRef](#)]
56. Friedman, A.E.; Kumar, C.V.; Turro, N.J.; Barton, J.K. Luminescence of ruthenium(II) polypyridyls: Evidence for intercalative binding to z-DNA. *Nucleic Acids Res.* **1991**, *19*, 2595.
57. Tan, C.; Lai, S.; Wu, S.; Hu, S.; Zhou, L.; Chen, Y.; Wang, M.; Zhu, Y.; Lian, W.; Peng, W. Nuclear permeable ruthenium(II) β -carboline complexes induce autophagy to antagonize mitochondrial-mediated apoptosis. *J. Med. Chem.* **2010**, *53*, 7613–7624. [[CrossRef](#)]
58. Tan, C.; Wu, S.; Lai, S.; Wang, M.; Chen, Y.; Zhou, L.; Zhu, Y.; Lian, W.; Peng, W.; Ji, L. Synthesis, structures, cellular uptake and apoptosis-inducing properties of highly cytotoxic ruthenium–norharman complexes. *Dalton Trans.* **2011**, *40*, 8611–8621. [[CrossRef](#)]
59. Qian, C.; Wang, J.-Q.; Song, C.-L.; Wang, L.-L.; Ji, L.-N.; Chao, H. The induction of mitochondria-mediated apoptosis in cancer cells by ruthenium(II) asymmetric complexes. *Metallomics* **2013**, *5*, 844–854. [[CrossRef](#)]
60. Jiang, G.-B.; Xie, Y.-Y.; Lin, G.-J.; Huang, H.-L.; Liang, Z.-H.; Liu, Y.-J. Synthesis, characterization, DNA interaction, antioxidant and anticancer activity studies of ruthenium(II) polypyridyl complexes. *J. Photochem. Photobiol. B Biol.* **2013**, *129*, 48–56. [[CrossRef](#)]
61. Mazuryk, O.; Maciuszek, M.; Stochel, G.; Suzenet, F.; Brindell, M. 2-Nitroimidazole-ruthenium polypyridyl complex as a new conjugate for cancer treatment and visualization. *J. Inorg. Biochem.* **2014**, *134*, 83–91. [[CrossRef](#)]
62. Griffith, C.; Dayoub, A.S.; Jaranatne, T.; Alatrash, N.; Mohamedi, A.; Abayan, K.; Breitbach, Z.S.; Armstrong, D.W.; MacDonnell, F.M. Cellular and cell-free studies of catalytic DNA cleavage by ruthenium polypyridyl complexes containing redox-active intercalating ligands. *Chem. Sci.* **2017**, *8*, 3726–3740. [[CrossRef](#)]
63. Gill, M.R.; Cecchin, D.; Walker, M.G.; Mulla, R.S.; Battaglia, G.; Smythe, C.; Thomas, J.A. Targeting the endoplasmic reticulum with a membrane-interactive luminescent ruthenium(II) polypyridyl complex. *Chem. Sci.* **2013**, *4*, 4512–4519. [[CrossRef](#)]
64. Audi, H.; Azar, D.; Mahjoub, F.; Farhat, S.; El-Masri, Z.; El-Sibai, M.; Abi-Habib, R.J.; Khnayzer, R.S. Cytotoxicity modulation of ruthenium(II) tris-bathophenanthroline complexes with systematically varied charge. *J. Photochem. Photobiol. A* **2018**, *351*, 59–68. [[CrossRef](#)]
65. Ison, A.; Xu, C.; Weakley, G.K.; Richardson, D.E. Catalytic autoxidations using tris-diimine iron(II) coordination complexes. *J. Mol. Catal. A Chem.* **2008**, *293*, 1–7. [[CrossRef](#)]

66. Ogawa, K.; Kobuke, Y. Recent advances in two-photon photodynamic therapy. *Anti-Cancer Agents Med. Chem.* **2008**, *8*, 269–279. [[CrossRef](#)]
67. Wilson, B.C.; Jeeves, W.P.; Lowe, D.M. In vivo and post mortem measurements of the attenuation spectra of light in mammalian tissues. *Photochem. Photobiol.* **1985**, *42*, 153–162. [[CrossRef](#)]
68. Castellano, F.N. Inorganic chemistry: Making iron glow. *Nature* **2017**, *543*, 627. [[CrossRef](#)]
69. Chábera, P.; Liu, Y.; Prakash, O.; Thyraug, E.; El Nahhas, A.; Honarfar, A.; Essén, S.; Fredin, L.A.; Harlang, T.C.; Kjær, K.S. A low-spin Fe(III) complex with 100-ps ligand-to-metal charge transfer photoluminescence. *Nature* **2017**, *543*, 695. [[CrossRef](#)]
70. Leonidova, A.; Pierroz, V.; Rubbiani, R.; Heier, J.; Ferrari, S.; Gasser, G. Towards cancer cell-specific phototoxic organometallic rhenium(I) complexes. *Dalton Trans.* **2014**, *43*, 4287–4294. [[CrossRef](#)]
71. Bruce, S.J.; Tavazzi, I.; Parisod, V.R.; Rezzi, S.; Kochhar, S.; Guy, P.A. Investigation of human blood plasma sample preparation for performing metabolomics using ultrahigh performance liquid chromatography/mass spectrometry. *Anal. Chem.* **2009**, *81*, 3285–3296. [[CrossRef](#)] [[PubMed](#)]
72. Bonnett, R.; Martinez, G. Photobleaching of sensitizers used in photodynamic therapy. *Tetrahedron* **2001**, *57*, 9513–9547. [[CrossRef](#)]
73. Mang, T.S.; Dougherty, T.J.; Potter, W.R.; Boyle, D.G.; Somer, S.; Moan, J. Photobleaching of porphyrins used in photodynamic therapy and implications for therapy. *Photochem. Photobiol.* **1987**, *45*, 501–506. [[CrossRef](#)] [[PubMed](#)]
74. Puckett, C.A.; Ernst, R.J.; Barton, J.K. Exploring the cellular accumulation of metal complexes. *Dalton Trans.* **2010**, *39*, 1159–1170. [[CrossRef](#)] [[PubMed](#)]
75. Puckett, C.A.; Barton, J.K. Methods to explore cellular uptake of ruthenium complexes. *J. Am. Chem. Soc.* **2007**, *129*, 46–47. [[CrossRef](#)] [[PubMed](#)]
76. Nakamaru, K. Solvent effect on the nonradiative deactivation of the excited state of tris(2,2'-bipyridyl)ruthenium(II) ion. *Bull. Chem. Soc. Jpn.* **1982**, *55*, 1639–1640. [[CrossRef](#)]
77. Kochevar, I.E.; Redmond, R.W. [2] Photosensitized production of singlet oxygen. In *Methods in Enzymology*; Academic Press: Cambridge, MA, USA, 2000; Volume 319, pp. 20–28.
78. Garcia-Fresnadillo, D.; Georgiadou, Y.; Orellana, G.; Braun, A.M.; Oliveros, E. Singlet-oxygen ($^1\Delta_g$) production by ruthenium(II) complexes containing polyazaheterocyclic ligands in methanol and in water. *Helv. Chim. Acta* **1996**, *79*, 1222–1238. [[CrossRef](#)]



© 2019 by the authors. Licensee MDPI, Basel, Switzerland. This article is an open access article distributed under the terms and conditions of the Creative Commons Attribution (CC BY) license (<http://creativecommons.org/licenses/by/4.0/>).